HHS Public Access

Author manuscript

Hepatology. Author manuscript; available in PMC 2019 December 01.

Published in final edited form as:

Hepatology. 2019 December ; 70(6): 2107–2122. doi:10.1002/hep.30677.

Mannose Phosphate Isomerase and Mannose Regulate Hepatic Stellate Cell Activation and Fibrosis in Zebrafish and Humans

Charles DeRossi[1], **Kathryn Bambino**[2], **Joshua Morrison**[1], **Isabel Sakarin**[1], **Carlos Villacorta-Martin**[3], **Changwen Zhang**[4], **Jillian L. Ellis**[4], **M. Isabel Fiel**[5], **Maria Ybanez**[6,7], **Youngmin A. Lee**[6], **Kuan-lin Huang**[8], **Chunyue Yin**[4], **Takuya F. Sakaguchi**[9], **Scott L. Friedman**[7], **Augusto Villanueva**[7], **Jaime Chu**[1]

[1]Department of Pediatrics, Icahn School of Medicine at Mount Sinai, New York, NY

[2]Department of Environmental Medicine and Public Health, Icahn School of Medicine at Mount Sinai, New York, NY

[3]Center for Regenerative Medicine, Boston University and Boston Medical Center, Boston, MA

[4]Division of Gastroenterology, Hepatology and Nutrition, Cincinnati Children's Hospital Medical Center, Cincinnati, OH

[5]Department of Pathology, Icahn School of Medicine at Mount Sinai, New York, NY

[6]Laboratory of RNA Molecular Biology, Rockefeller University, New York, NY

[7]Division of Liver Diseases, Department of Medicine, Icahn School of Medicine at Mount Sinai, New York, NY

[8]Department of Genetics and Genomic Sciences, Icahn School of Medicine at Mount Sinai, New York, NY

[9]Department of Stem Cell Biology and Regenerative Medicine, Lerner Research Institute, Cleveland Clinic Foundation, Cleveland, OH

Abstract

The growing burden of liver fibrosis and lack of effective antifibrotic therapies highlight the need for identification of pathways and complementary model systems of hepatic fibrosis. A rare, monogenic disorder in which children with mutations in mannose phosphate isomerase (MPI) develop liver fibrosis led us to explore the function of MPI and mannose metabolism in liver development and adult liver diseases. Herein, analyses of transcriptomic data from three human liver cohorts demonstrate that *MPI* gene expression is down-regulated proportionate to fibrosis in chronic liver diseases, including nonalcoholic fatty liver disease and hepatitis B virus. Depletion of MPI in zebrafish liver *in vivo* and in human hepatic stellate cell (HSC) lines in culture activates

ADDRESS CORRESPONDENCE AND REPRINT REQUESTS TO: Jaime Chu, M.D., Department of Pediatrics, Icahn School of Medicine at Mount Sinai, 1 Gustave L. Levy Place, Box 1104, New York, NY 10029 jaime.chu@mssm.edu Tel.: +1-212-659-8060.

Potential conflict of interest: Dr. Villanueva has received consulting fees from Guidepoint and Fujifilm Wako; advisory board fees from Exact Sciences, Nucleix and NGM; and lecture fees from Exelixis.

Supporting Information

Additional Supporting Information may be found at onlinelibrary.wiley.com/doi/10.1002/hep.30677/suppinfo.

fibrotic responses, indicating that loss of MPI promotes HSC activation. We further demonstrate that mannose supplementation can attenuate HSC activation, leading to reduced fibrogenic activation in zebrafish, culture-activated HSCs, and in ethanol-activated HSCs.

Conclusion: These data indicate the prospect that modulation of mannose metabolism pathways could reduce HSC activation and improve hepatic fibrosis.

The dearth of effective antifibrotic therapies highlights the need for identification of pathways and complementary model systems of hepatic fibrosis. Activation of hepatic stellate cells (HSCs) is central to liver fibrosis and is the main focus of antifibrotic drug discovery efforts. The functional contribution of glycosylation pathways to HSC activation and fibrosis has been largely overlooked.

Children with a congenital disorder of glycosylation (CDG) who lack the enzyme, mannose phosphate isomerase (MPI), have altered protein glycosylation and develop early, progressive liver fibrosis requiring transplantation.[1–3] This monogenic disease poignantly demonstrates that loss of MPI provokes liver fibrosis; however, the mechanisms underlying this effect are not known. MPI interconverts fructose 6-phosphate and mannose 6-phosphate (Fru6P ⟷ Man6P; Supporting Fig. S1), key intermediates in glycolysis and protein N-linked glycosylation, respectively. Importantly, mannose supplements can bypass MPI deficiency and directly provide Man6P for glycan synthesis (Supporting Fig. S1), leading to improvement in almost all symptoms within a few weeks.[4,5] We previously established a zebrafish model of MPI-CDG with clinical cornerstones similar to MPI-CDG, including phenotypic rescue with mannose supplementation.[6] Here, we utilize this model to investigate how loss of MPI leads to liver fibrosis *in vivo* and, more broadly, explore the potential contribution of reduced MPI in common adult fibrotic liver diseases. This disorder provides a unique opportunity to study the molecular basis of an early form of hepatic fibrosis, because the underlying genetic defect is clearly established.

HSC activation is a central event in response to chronic hepatocyte injury, leading to secretion of collagen and other extracellular matrix (ECM) proteins that promote development and progression of liver fibrosis to cirrhosis.[7] Drug discovery efforts to target hepatic fibrosis have focused on known pathways and regulators of HSC activation, yet few candidates have entered early-phase clinical trials, and none have been approved for treatment.[7] Based on initial studies in zebrafish, we hypothesized that loss of MPI in HSCs can amplify their activation, even in the presence of little or no liver injury.

Here, we investigate the broader role of MPI and mannose metabolism in liver development and adult liver diseases and integrate findings using human liver samples, *in vivo* zebrafish models, and HSCs in culture to investigate an important role of MPI and mannose in regulating HSC activation and hepatic fibrosis. By extrapolating therapy from a rare disease, our data suggest that mannose supplementation could potentially be a simple and effective antifibrotic therapy that merits further evaluation.

Materials and Methods

ZEBRAFISH MAINTENANCE, INJECTION, AND TREATMENT OF EMBRYOS

Procedures were performed in accord with the Icahn School of Medicine at Mount Sinai (ISMMS) Institutional Animal Care and Use Committee. Adult fish were maintained on a 14:10 light/dark cycle at 28°C. Wild-type (WT; AB and Tab 14), *Tg(fabp10a: nls-mcherry)*^{mss4}[8], *Tg(hand2:EGFP)*^{pd24},[9] *Tg(TP1: βglobin-GFP)*^{um14},[10] *Tg(kdrl:ras-mCherry)*^{s896},[11] and *mpi*^{mss7}[12] zebrafish strains were used. Fertilized embryos were collected and cultured in fish water (0.6 g/L of Crystal Sea Marinemix; Marine Enterprises, Baltimore, MD) containing methylene blue and maintained at 28°C. Embryos were injected with 4 ng of standard control or *mpi* morpholino[6] at the one-to four-cell stage. Embryos were treated with D-mannose or 2% ethanol as described.[6,13]

HISTOLOGY

Whole livers were dissected from 19-month-old, male adult zebrafish and fixed overnight at 4°C in Bouin's fixative. Four-micron serial sections of paraffin-embedded fish were stained with Masson's trichrome and imaged on an Olympus BX41 microscope (Olympus Corporation, Waltham, MA) and Nikon DS-Ri1 digital camera (Nikon Instruments, Inc., Melville, NY).

IMMUNOFLUORESCENCE

Zebrafish were fixed in 4% paraformaldehyde (PFA) in phosphate-buffered saline (PBS) overnight at 5 days postfertilization (dpf) and transferred to 30% sucrose in PBS overnight. Larvae were embedded in optimum cutting temperature (OCT) compound (Tissue-Tek), and 10-μm serial sections were obtained using the Leica CM3050 S Research Cryostat. Sections were washed in PBS + 0.1% Tween-20 (PBST). Tissue sections were blocked with 5% fetal bovine serum (FBS) and 2% bovine serum albumin (BSA) in PBST for 1.5 hours at room temperature (RT). A custom polyclonal antibody recognizing zebrafish Mpi was commercially prepared in rabbit (Biomatik, Inc, Wilmington, DE) using the sequence DPQAHIEHSKPYAE as the target antigen. Sections were stained with *Mpi* antibody (1:200) overnight at 4°C and then with 1:250 goat antirabbit Alexa Fluor 488 (A11008; Life Technologies, Waltham, MA) for 1.5 hours in the dark at RT. Sections were mounted with ProLong Gold Antifade Mountant with 4′,6-diamidino-2-phenylindole (DAPI; Life Technologies) and imaged using a Leica SP5 DMI at 63×. Biliary network reconstruction was performed as described.[14] Mouse liver sections (Lrat-CRE/ZsGreen$^{Flox/Flox}$)[15] were fixed in 4% PFA in PBS overnight and incubated for 24 hours each in 10%, 20%, and then 30% sucrose in PBS before embedding in OCT, and sectioned in 10 μM. Tissue sections were rehydrated in PBS and incubated with anti-MPI antibody (Sigma SAB2700835, 1:100; Sigma-Aldrich, St. Louis, MO), anti-CD31 antibody (550274, 1:200; BD Pharmingen, San Jose, CA), and anti–glial fibrillary acidic protein (GFAP; ab4674, 1:200; Abcam, Cambridge, MA) diluted in PBS overnight at 4°C. Sections were washed with PBS and incubated with appropriate secondary antibodies (A10520, A11007, A21245, and A21437; ThermoScientific, Waltham, MA) at 1:500 in PBS for 1 hour at RT. Sections were washed 3× in PBS and mounted in DAPI Fluoromount-G Mounting Medium (SouthernBiotech, Birmingham, AL). Imaging was performed on a Zeiss Axio Observer 7 (Zenblue software).

CELL CULTURE

TWNT-4 and LX-2 human HSC lines[16,17] were maintained in complete medium (Dulbecco's modified Eagle's medium [DMEM] supplemented with 10% FBS and L-glutamine) and routinely tested for mycoplasma using the Venor GeM Mycoplasma Detection Kit (Sigma-Aldrich). For MPI knockdown experiments, small interfering RNAs (siRNAs) targeting human *MPI* (siMPI; see a previous work[12]) were transfected using Lipofectamine RNAiMAX transfection reagent (ThermoFisher, Waltham, MA), following the recommended protocol. Cells were collected 48 hours after transfection for total RNA or protein. For ethanol and mannose treatments, cells were grown in complete medium, replaced with starvation medium (DMEM + 0.1% BSA and 2 mM of L-glutamine) overnight (16–20 hours), replaced with starvation medium supplemented without or with ethanol and mannose, as described in the text, and collected 24 hours later for total RNA or protein. For proteomics analysis, man-nose-treated or untreated LX-2 cells were collected by scraping in 8 M of urea/20 mM of Hepes buffer (pH 7.1) with phosphatase inhibitors (Roche PhosSTOP, Sigma-Aldrich). Like samples (10 mL total) were combined, flash-frozen, and stored at –80°C until processing.

TRICHLORACETIC ACID PRECIPITATION OF MEDIA PROTEIN

Conditioned media were collected from cultures, and media proteins were precipitated with an equal volume of ice-cold 10% trichloracetic acid (TCA) for 1–2 hours on ice, centrifuged, and washed with ice-cold acetone for 30 minutes on ice and centrifuged again. Protein pellets were resuspended in nonidet P-40 (NP-40) cell lysis buffer (50 mM of Tris.Cl [pH 8.0], 150 mM of NaCl, and 1% NP-40) + protease inhibitor (Roche Complete, Sigma-Aldrich) to achieve 5× concentration and sonicated to resuspend. Twenty microliters of concentrate were separated by sodium dodecyl sulfate/polyacrylamide gel electrophoresis (SDS-PAGE) for analysis.

MPI ENZYME ACTIVITY ASSAY

MPI activity assay was performed according to our published protocol in zebrafish and mammalian cells extract.[6,12] Briefly, zebrafish or cell lysates were homogenized and MPI activity was assessed in 15 ug of protein extract using a coupled-fluorometric assay.

GENE EXPRESSION ANALYSIS IN ZEBRAFISH LIVERS AND HUMAN CELL LINES

Livers were microdissected from anesthetized zebrafish larvae and collected in 20 μL of RLT Buffer (Qiagen, Germantown, MD). Total RNA was isolated from >10 livers per sample by TRIzol extraction (Life Technologies). Human HSCs were lysed in TRIzol, following the supplied protocol. RNA was reverse transcribed using the SuperScript complementary DNA (cDNA) synthesis kit (Quantabio, Beverly, MA). qRT-PCR was performed using PerfeCTa SYBR Green Fast Mix (Quantabio). Samples were run in triplicate on the Roche LightCycler 480 in a reaction volume of 10 μL. Gene expression levels were normalized to ribosomal protein large P0 (zebrafish) or ribosomal protein S18 (human) using the comparative threshold cycle (ΔΔCt) method. Primer sequences are listed in Supporting Table S1.

Human Samples (*In Silico*)

To assess the association of MPI depletion and fibrosis in human chronic liver disease, we selected three different cohorts of human samples, which encompass different degrees of fibrosis and two etiologies for which genome-wide expression data are available: hepatitis B virus (HBV; ArrayExpress E-GE0D-84044); nonalcoholic fatty liver disease (NAFLD; see a previous work[18], E-GEOD-49541); and Heptromic (see a previous work[19], GEO Omnibus GSE63898). In the HBV cohort, patients were categorized in two groups according to their Scheuer staging (i.e., scarring and architectural distortion): low (value ≤ 2) and high (value > 2). Differences in MPI expression were tested with the Mann-Whitney U test. Subsequent functional characterization of samples with various MPI expression levels was studied using gene set enrichment analysis (GSEA; also see a previous work[20]). We ranked patients based on MPI expression level (regardless of their Scheuer staging and grading) and compared the expression of all genes for patients <10th percentile in MPI expression with those >90th percentile. Differentially expressed genes were identified using linear models as implemented in the limma package,[21] and *P* values were corrected for multiple testing using the Benjamini-Hochberg procedure. Volcano plots show data of one probe per gene. For those genes with multiple probes, the one with the highest fold-change expression is depicted in the plot. The resulting fold changes were used to rank the genes and test enrichment of Kyoto Encyclopedia of Genes and Genomes (KEGG) pathways using GSEA.[20] The NAFLD cohort was analyzed in a similar way, with the patients categorized by degree of fibrosis: advanced NAFLD (stages 3 and 4) versus mild NAFLD (stages 0 and 1). For this cohort, because the total number of patients was significantly lower than for the other two data sets, we compared expression between patients with MPI values <35th percentile and those with >65th percentile. In the Heptromic cohort, the comparison was made between normal liver samples and adjacent cirrhotic tissues from patients with hepatocellular carcinoma (HCC). The rest of the analyses are analogous to the HBV cohort.

WESTERN BLOTTING

Zebrafish samples were homogenized in lysis buffer (20 mM of Tris [pH 7.5], 150 mM of NaCl, 1% NP-40, 2 mM of ethylenediaminetetraacetic acid, 10% glycerol, 1% β-mercaptoethanol, and protease inhibitors [Roche Complete]). Lysates were centrifuged with one volume sample buffer added to each sample. Cell samples were collected by trypsinization and lysed by sonication in NP-40 cell lysis buffer + protease and phosphatase (Roche PhosSTOP) inhibitors. Lysates were resolved by 12% SDS-PAGE. Anti-PDGFRB (sc-432 at 1:1,000; Santa Cruz Biotechnologies, Dallas, TX), anti–Collagen 1a (BS-10432R at 1:1,000; Bioss, Woburn, MA), and anti-Tubulin (12G10 at 1:2,000; DSHB, Iowa City, IA) were used.

PROTEOMICS ANALYSIS

Urea lysates from mannose-treated or untreated LX-2 cells were processed for proteomic analysis by the Stony Brook University (SBU) Biological Mass Spectrometry Shared Resource Facility. Briefly, samples were reduced, alkylated, proteolytically cleaved, and desalted using C18 Sep-Pak Plus Cartridges (Waters WAT020515). On-column peptides were desalted and eluted with sequential 10%, 20%, and 50% acetonitrile, 0.1%

trifluoroacetic acid, and lyophilized. Phospho-and total peptide fractions were isolated and labeled with isobaric tagging for relative and absolute quantitation (iTRAQ) stable isotope tags (Sigma 4381662), run on a Sciex 5600+ quad-rupole quantitative time-of-flight liquid chromatography with tandem mass spectrometry instrument, and analyzed using Analyst QS 1.1 to determine peptide masses, sequence information, and abundance. For differentially regulated pathway analysis, we first calculated the ratio of protein or phosphoprotein in Mannose-treated versus control experiments and then selected the experimental replicate with the highest number of observed protein or phosphoprotein for downstream analyses. For phosphoproteomics data, we collapsed the phosphosites to gene-level phosphorylation values by averaging the phosphosite expressions observed for each protein. We used the Wilcoxon rank-sum test to test for changes in protein expression or phosphorylation ratio ranks of members in each KEGG signaling pathway against all the other observed protein in that sample. Resulting *P* values were adjusted using the Benjamini-Hochberg procedure to false discovery rate (FDR).

STATISTICAL ANALYSIS

Data were analyzed using GraphPad Prism software (version 8; GraphPad Software Inc., San Diego, CA). Data are expressed as mean ± SD. Differences between experimental and control groups were analyzed by two-tailed, paired Student *t* test or one-way analysis of variance, followed by Dunnet's or Tukey's post-hoc correction, when more than two groups were compared. *P* values <0.05 were considered statistically significant.

RESULTS

MPI EXPRESSION IS INVERSELY CORRELATED WITH ADVANCED FIBROSIS IN HUMAN LIVER DISEASE

MPI loss leads to early fibrosis in children with MPI-CDG, suggesting a link between MPI deficiency and liver fibrosis. To determine whether changes in MPI correlated with common etiologies of liver disease, we analyzed publicly available transcriptome expression data sets encompassing fibrotic samples from three human liver disease cohorts totaling 376 samples and arising from different etiologies: HBV cohort (n = 124), NAFLD cohort (n = 72), and the Heptromic cohort (normal liver and cirrhotic samples of multiple etiologies, HCC samples excluded; n = 180). In all three cohorts, *MPI* was significantly down-regulated in samples with advanced fibrosis (Fig. 1A), regardless of the etiology. We found significant heterogeneity in expression values of *MPI* across tissues, suggesting that MPI is not the only factor contributing to this phenotype. Samples with low expression levels of *MPI* were enriched in fibrotic genes, such as collagen type I alpha 1 chain (*COL1A1*), collagen type IV alpha 3 chain, and collagen type I alpha 2 chain (Fig. 1B; Supporting Table S2). GSEA in samples with low *MPI,* regardless of level of fibrosis, revealed cell and focal adhesion clusters to be consistently ranked first among the gene sets significantly enriched in these samples across data sets (Fig. 1C; Supporting Table S3), a finding consistent with deranged cell adhesion as a hallmark of liver fibrosis.[22] These data demonstrate an inverse correlation between *MPI* gene expression and fibrosis in adult human liver disease.

MPI LOSS BLOCKS HEPATIC DEVELOPMENT IN ZEBRAFISH

Zebrafish are an excellent system to study liver development and disease, including steatosis, fibrosis, and liver cancer.[23] We previously established a zebrafish model of *Mpi* depletion using morpholino oligonucleotides (MOs), which led to a significant decrease in Mpi enzymatic activity and hallmarks of hypoglycosylation comparable to those of MPI-CDG patients.[6] To use this model to study the role of MPI in liver disease, we first confirmed that Mpi is abundantly expressed in zebrafish liver using a custom antibody raised against zebrafish Mpi, followed by immunofluorescent imaging in a transgenic line that expresses a fluorescent protein under a hepatocyte-specific promoter, *Tg(fabp10a:nls-mCherry)*[8] (Supporting Fig. S2A). To assess for potential liver defects following Mpi loss, Mpi was efficiently depleted in this transgenic line using morpholino targeting as described[6] (Supporting Fig. S2B). Severity of the whole-body phenotype in *Tg*(*fabp10a:nls-mCherry*) larvae correlated with Mpi activity and protein level (Fig. 2A,B and Supporting Fig. S2B). Importantly, consistent with our previous reports,[6] *mpi* morphants developed smaller livers, which also correlated with severity of whole-body phenotype (Fig. 2C), suggesting a link between acute Mpi depletion and liver pathology. In addition, using a transgenic reporter for Notch activity to identify biliary cells (*Tg(TP1:βglobin-GFP)*)[10] *mpi* morphants developed an abnormal biliary system characterized by dilated branches of the biliary tree compared to control livers (Fig. 2D,E).

We have previously reported on the overt *mpi* MO phenotype and did not identify defects that are suggestive of delayed embryonic development.[6] However, to determine whether biliary abnormality was secondary to overall developmental delay, we quantified biliary length as a measure of developmental progression, and despite the abnormal branching, we found similar lengths between *mpi* morphants and controls (Supporting Fig. S2C). Furthermore, Annexin A4 staining with 2F11 antibody[24] identified the presence of differentiated cholangiocytes in *mpi* MO livers at 100 high-power field (hpf; Supporting Fig. S2D), at which point full differentiation and development of well-defined ducts are complete.[25] These data demonstrate the capacity for biliary cell differentiation in these livers, and suggest that biliary phenotypes are not attributed to global developmental delay. Together, these findings show that Mpi depletion in zebrafish larvae causes developmental defects in the liver, including small liver size and abnormal biliary development.

LOSS OF MPI ACTIVATES HSCs AND PROMOTES FIBROGENESIS

HSCs are the main driver of fibrosis, so we examined whether reduction of MPI is sufficient to drive HSC activation. Using a zebrafish transgenic reporter line for HSCs (*Tg(hand2:EGFP)*[9]), we first confirmed Mpi expression in zebrafish HSCs using immunofluorescence and found that Mpi colocalized with Hand2 (Fig. 3A). However, there was no difference in total HSC number between control and *mpi* morphants at 5 dpf, as calculated by the HSC/DAPI ratio (Supporting Fig. S3A–SC). To investigate the effects of MPI loss on HSC activation, we isolated livers from control and *mpi* MO embryos at 5 dpf and used qRT-PCR to measure expression of genes reflecting activation of fibrotic response.[26] Gene expression for the ECM proteins, collagen, type I, alpha 1b *(col1a1b),* actin, alpha 2, smooth muscle (*acta2*), platelet-derived growth factor receptor beta (*pdgfrb*), laminin subunit beta 4A *(lamb4a), and* tissue inhibitor of metalloproteinases 2 (*timp2b*), were

significantly increased in *mpi* MO livers (Fig. 3B). There was no induction of transforming growth factor beta 1 (*tgfb1*) or platelet-derived growth factor subunit B (*pdgfb;* Fig. 3B), which encode growth factor ligands secreted by hepatocytes and biliary cells to induce HSC activation and proliferation[27] This suggested autonomous induction of HSCs following MPI depletion, which was not dependent on hepatocyte interactions. We previously established an *mpi* mutant zebrafish line (ZFIN:*mpi*^{mss7}),[12] in which residual Mpi activity at 5 dpf is comparable to that found in MPI-CDG patients with hypomorphic mutations[6,12] Like the embryonic lethal phenotype of *mpi* morphants, homozygous *mpi*$^{mss7/mss7}$mutants do not survive larval development.[12] Therefore, to determine whether a sustained fibrogenic effect persisted past embryonic development and into adult stages, we analyzed livers from *mpi*$^{+/mss7}$ heterozygous adults (liver Mpi activity 69%; Supporting Fig. S3D). The mild Mpi depletion in heterozygous mutants demonstrated a persistent elevation in many fibrogenic genes at >1 year, including *pdgfrb,* collagen, type I, alpha 1a *(col1a1a), col1a1b,* and *acta2* (Fig. 3C). Heterozygous mutant adult livers were sectioned and stained with Masson trichrome to visualize collagen as an indicator of fibrosis. Heterozygous mutant adult livers demonstrated abnormal bile ducts embedded within fibrotic stroma when compared to age-and sex-matched WT siblings with no fibrosis and normal bile duct profiles (Fig. 3D). These results suggest that even subtle loss of Mpi is correlated with increased fibrosis, and, collectively, that both acute and chronic loss of Mpi *in vivo* is sufficient to induce a sustained fibrogenic response in zebrafish liver during development and in adulthood.

Because our transcriptomic analysis of HBV and NAFLD liver tissues demonstrated a correlation between lower *MPI* levels and worsened fibrosis, we asked whether Mpi depletion may sensitize the liver to injury and fibrosis *in vivo.* To test this, we treated zebrafish embryos from either WT or *mpi*$^{+/mss7}$ heterozygous adult incrosses (pooled embryos with 58% average Mpi activity[12]) with 2% ethanol from 96 to 120 hpf.[13,26] Livers with Mpi depletion demonstrated a clear trend toward induction of fibrogenic genes (*col1a1a, acta2, pdgfrb,* and *timp2b*), but not for ligands *tgfb1a* or *pdgfb,* when treated with 2% ethanol, compared to ethanol-treated WT embryos (Supporting Fig. S4). These results suggest that loss of Mpi may exacerbate the fibrogenic response to known stressors such as ethanol, HBV, or NAFLD.

We next explored whether MPI depletion promotes fibrogenesis through direct activation of human HSCs. First, we verified that MPI is expressed in mammalian HSCs. We found MPI to be highly expressed in mammalian HSCs using immunofluorescence for the HSC marker, GFAP,[28] in normal mouse liver tissue (Fig. 4A), as well as robust MPI protein expression in human HSCs, as visualized by western blotting (Supporting Fig. S5A). In addition to HSCs, MPI expression was found in other liver cell types, including hepatocytes and liver sinusoidal endothelial cells (Supporitng Figs. S5B and S6). To determine the effects of MPI loss in HSCs, MPI was depleted in the human LX-2 HSC line using a specific siRNA against human *MPI* (MPI activity depleted to 44% of control). Downstream transcriptional responses were characterized through qRT-PCR. MPI depletion in these cells increased expression of *COL1A1* and *PDGFRB,* whereas *ACTA2* expression was unchanged (Fig. 4B). Similar to *Mpi-depleted* zebrafish whole livers, *PDGFB* and *TGFB* ligand expression remained unchanged from controls (Fig. 4B). These results were confirmed by depleting

MPI using short hairpin RNA in LX-2 cells, which resulted in increased expression of *COL1A1, PDGFRB,* and *ACTA2* (Supporting Fig. S5C–E). In addition, COL1A levels were increased in media from MPI-depleted HSCs compared to controls (Fig. 4C), suggesting that loss of MPI leads to enhanced HSC secretion of matrix protein COL1A to drive fibrosis. Changes in fibrogenic gene expression observed in MPI depletion were found to be in similar ranges to that of standard TGFB activation with the exception of *ACTA2*, and ligands *PDGFB* and *TGFB* (Fig. 4B), suggesting a potential difference in mechanism of HSC activation.

Given the expression of MPI in hepatocytes (Supporting Figs. S5B and S6A), we next investigated the paracrine effects of MPI depletion in hepatocytes on HSC activation. Cell mixing experiments demonstrated that the increased expression of fibrogenic genes in MPI-depleted LX-2 cells was neither significantly enhanced by conditioned media from MPI-depleted hepatocyte cultures (THLE5B and Huh7 cells; Supporting Fig. S7), nor did conditioned media induce HSC activation alone, suggesting that MPI loss directly activates HSCs (Supporting Fig. S7). These data demonstrate that acute and sustained MPI depletion are sufficient to activate HSCs and induce fibrogenesis in human HSC cells *in vitro* and in a whole vertebrate model.

MANNOSE SUPPRESSES HSC ACTIVATION AND FIBROSIS

Our data point to a role for MPI in HSC activation and liver fibrosis. Mannose supplementation is the standard treatment for MPI-CDG and works by directly producing Man6P by phosphorylation, bypassing MPI deficiency (Supporting Fig. S1).[4] Based on results of therapy for MPI-CDG, we explored whether mannose supplementation attenuated liver phenotypes *in vivo* in zebrafish, and whether mannose reduced human HSC activation in culture. We have previously shown that mannose can rescue the *mpi* MO phenotype, including restoration of liver size. Therefore, we treated *Mpi*-depleted zebrafish embryos with 50 mM of D-mannose immediately following morpholino injection and assessed expression of profibrotic genes in the liver. Mannose mitigated induction of fibrogenic genes (except *col1a1a)* in Mpi-deficient zebrafish (Fig. 5A), demonstrating that early mannose supplementation is effective at protecting against fibrosis in the zebrafish model of MPI-CDG.

Building upon the findings in zebrafish, we sought to determine whether mannose regulates human HSC activation. We treated two independent, serum-activated human HSC cell lines with increasing concentrations of D-mannose and assessed expression of fibrogenic genes. After 24 hours of treatment, there was a dose-dependent effect, with 1 mM of mannose more effective than 0.25 mM of mannose, but with an effective plateau or saturation at concentrations higher than 1 mM (Fig. 5B,C). These data demonstrate a role for mannose supplementation in attenuating fibrogenic gene expression in culture-activated human HSCs in a concentration-dependent manner.

We next asked whether mannose treatment was effective against a clinically relevant inducer of hepatic fibrosis using ethanol, a potent activator of human HSCs.[29] Serum-starved LX-2 cells were treated with ethanol across a range of mannose concentrations. Untreated cells produced very little COL1A1 or PDGFRB, but, as expected, both fibrotic markers were

strongly induced upon exposure to 50 mM of ethanol for 24 hours (Fig. 5D). Remarkably, cotreatment with mannose mitigated the induction of these fibrogenic markers, in a dose-dependent manner (Fig. 5D).

To investigate pathways altered in mannose-mediated HSC attenuation, we performed unbiased proteomics analysis using iTRAQ with LX-2 cells treated with and without 1 mM of mannose supplementation (n = 2 replicates per group). Among the differentially regulated pathway analysis of total proteins and of phosphoproteins in mannose-treated versus control experiments, glycolysis and glutamate metabolism were among the top pathways altered in HSCs treated with mannose (Table 1). Regulation of glucose and glutamine metabolism are both important for HSC activation based on these data and previous studies.[30,31] Together, our data suggest a model whereby reduction of MPI, either through an endogenous genetic mutation or during the process of HSC activation, is sufficient to promote HSC activation and indicate an antifibrotic role for mannose supplementation in HSC attenuation.

Discussion

Here, we focus on MPI as an important mediator of HSC activation and extrapolate therapies from this rare disease to clarify mechanisms of HSC activation. *In silico* analysis of human fibrosis samples ranging from HBV to NAFLD demonstrate an inverse correlation between *MPI* expression and fibrosis stage across etiologies. To further dissect this relationship, we have used the zebrafish as a whole-animal model in which we can modulate the mannose metabolism pathway.[6] Mpi depletion in zebrafish results in hepatic fibrosis and biliary defects, similar to those observed in humans with *MPI* mutations. Our finding that mannose, a simple hexose sugar, mitigates the fibrotic response in culture-activated and ethanol-treated HSCs to suggest that inhibition of this enzyme may contribute to fibrosis, but that a simple treatment with mannose could possibly reverse it.

Zebrafish livers showed a more robust induction of fibrogenic gene expression in response to MPI loss than HSCs in culture (Figs. 3 and 4). HSCs comprise ~10% of resident liver cells,[32] and it is possible that systemic loss of MPI can have effects on non-HSC liver cells given that *mpi* morphant livers are smaller than livers in control siblings. *mpi* morphant livers contained abnormal vasculature, as marked by expression of *Tg(kdrl:ras-mCherry)* and measured by vessel branches per liver area (Supporting Fig. S3E). Our data suggest that a cell-autonomous activation of HSCs is, at least partially, responsible for this phenotype, because there was no induction of *tgfb1* or *pdgfb* ligands in whole zebrafish livers from *mpi* morphants or $mpi^{+/mss7}$ adults, or MPI-depleted human HSCs (Figs. 3B,C and 4B, respectively). In addition, conditioned media from MPI-depleted hepatocytes did not induce a fibrogenic response in normal HSCs and did not exacerbate the effect of MPI knockdown in HSCs transfected with siMPI (Supporting Fig. S7). However, there are other paracrine growth factors that may contribute, and future studies clarifying which cell type(s) contribute to MPI-and mannose-mediated fibrotic changes are important. Another possibility is that, *in vivo*, MPI depletion leads to developmental defects stemming from a failure to remodel the developing biliary tree, which initiates liver fibrosis. In this case, conditional deletion of MPI may be used to understand its role in biliary development.

Previously published transcriptomic analysis of fibroblasts from multiple CDGs demonstrated increased expression of genes encoding ECM proteins compared to control fibroblasts.[33] Consistent with these data, our transcriptomic analysis of low-*MPI* human liver fibrosis samples and MPI-depleted HSC and zebrafish liver tissues demonstrated similar affected genes and pathways. These findings could implicate loss of protein glycosylation as an initiating event in fibrogenic response or, alternatively, suggest another function of MPI in fibrosis. Whereas many proteins are affected when protein hypoglycosylation is reduced, one pathway that merits further study is platelet-derived growth factor (PDGF) signaling, which is the most potent mitogenic driver of HSCs.[34] PDGF signaling is directly increased by loss of glycosylation—PDGFB is glycosylated and blocking its glycosylation increases PDGFB levels at the cell surface, leading to enhanced receptor binding and mitogenic activity.[35] Alternatively, aberrant glycosylation in PDGFB could result in improved presentation of the receptor-binding interface to PDGFRB to promote PDGF signaling.[35] Thus far, these studies have only been carried out *in vitro*, and the mechanisms and impact of altered glycosylation in PDGF signaling and HSC activation *in vivo* require further investigation.

As an alternative proposed mechanism, MPI reduction may activate HSCs through alterations in glycolysis and inter-related biosynthetic pathways. Recent studies have demonstrated increased bio-energetic and biosynthetic demands required for HSC activation dependent on glycolysis and glutaminolysis, given that blocking either of these pathways halts HSC activation.[30,31] Unbiased proteomics analysis suggests that these same pathways are altered in mannose supplementation of HSCs with decreased activation. Our group has indicated that MPI is a regulator of Warburg metabolism and directs glycolytic intermediates into the hexosamine biosynthetic pathway,[12] a key metabolic pathway which requires both glucose and glutamine as fuel. Recent publications demonstrate that mannose supplementation *in vivo* can suppress tumor cell proliferation[36] and steatosis.[37] Mannose may function similarly to suppress HSC activation through enhancing cell death or through changes in energy metabolism. Ongoing studies are examining the role of MPI and mannose in generating key substrates required for HSC activation and proliferation.

MPI-CDG patients receive oral mannose supplements to produce Man6P in order to bypass MPI deficiency (Supporting Fig. S1). Remarkably, mannose supplementation ameliorates most symptoms with restoration of glycosylation status of marker glycoproteins,[4,5] but, in some cases, liver fibrosis continues to progress.[3] Potential explanations for this lack of therapeutic response include: (1) irreversible, prolonged liver damage *in utero* and delay in diagnosis (MPI-CDG is often diagnosed well after infancy); (2) a nonglycosylation function of MPI and mannose therapy; or (3) higher doses of mannose are required to reverse the fibrosis. Current therapeutic guidelines for oral mannose supplements to treat MPI-CDG range from 0.1 to 1.0 g/kg of body weight daily and has been demonstrated in MPI-CDG patients to result in dose-dependent serum mannose concentrations of 250–490 μM.[1,3–5] In our study, this concentration has little effect on HSC expression of fibrogenic genes in culture (Fig. 5). However, mannose of ≥1 mM significantly reduced fibrogenic gene expression, suggesting that increasing the dosage of mannose supplements may have a beneficial effect on mitigating liver fibrosis and may be effective as an antifibrotic more generally.

This study indicates a role for glycosylation in HSC activation and underscores the potential of glycosylation in liver fibrosis. Most important, we integrate findings using zebrafish *in vivo* models, HSCs in culture, and *in silico* analysis of human fibrotic liver samples. Together, the data indicate that MPI loss is a driver of liver fibrosis and suggest that modulating mannose metabolism pathways could reduce HSC activation and improve hepatic fibrosis.

Supplementary Material

Refer to Web version on PubMed Central for supplementary material.

Acknowledgment:

We thank Dipankar Bhattacharya at ISMMS and Kirsten C. Sadler at New York University Abu Dhabi for their helpful discussions and reagents. We thank Nataly Shtraizent for her technical contributions. We thank the Pathology CoRE and Center for Comparative Medicine and Surgery at ISMMS, Confocal Imaging Core at CCHMC, and the SBU Proteomics Center.

Supported by K08 DK101340, Gilead Liver Research Scholars Award, Art in Giving/The Rachel Molly Markoff Foundation, and The Mindich Child Health and Development Institute at the Icahn School of Medicine at Mount Sinai to J.C., R01 DK 056221 to S.L.F., T32 HD049311 to K.B., and T32 AI078892 and T32 DK007792 to C.D. A. V. is the recipient of the American Association for the Study of Liver Diseases Foundation (AASLDF) Alan Hofmann Clinical and Translational Award, and he is supported by the U.S. Department of Defense (CA150272P3) and the Tisch Cancer Institute (Cancer Center Grant P30 CA196521). C.Z. is supported by an Arnold W. Strauss Fellow Award. C.Y. is supported by National Institutes of Health Grant R00 AA020514.

Abbreviations:

ACTA2	actin, alpha 2, smooth muscle
CDG	congenital disorders of glycosylation
cDNA	complementary DNA
COL1A1	collagen type I alpha 1 chain
col1a1a	collagen, type I, alpha 1a
col1a1b	collagen, type I, alpha 1b
dpf	days postfertilization
DA PI	4’,6-diamidino-2-phenylindole
ECM	extracellular matrix
FBS	fetal bovine serum
FDR	false discovery rate
GFAP	glial fibrillary acidic protein
GSEA	gene set enrichment analysis
HBV	hepatitis B virus

HSC(s)	hepatic stellate cell(s)
ISMMS	Icahn School of Medicine at Mount Sinai
lamb4a	laminin subunit beta 4A
Man6P	mannose 6-phosphate
MO	morpholino oligonucleotide
MPI	mannose phosphate isomerase
NAFLD	nonalcoholic fatty liver disease
NP-40	nonidet P-40
PBS	phosphate-buffered saline
PDGF	platelet-derived growth factor
PDGFB	platelet-derived growth factor subunit B
PDGFRB	platelet-derived growth factor receptor beta
RT	room temperature
siMPI	small interfering RNAs targeting human MPI
TGFB	transforming growth factor beta
tgfb1	transforming growth factor beta 1
timp2b	tissue inhibitor of metalloproteinases 2
WT	wild type

REFERENCES

1). Janssen MC, de Kleine RH, van den Berg AP, Heijdra Y, van Scherpenzeel M, Lefeber DJ, Morava E. Successful liver transplantation and long-term follow-up in a patient with MPI-CDG. Pediatrics 2014;134:e279–e283. [PubMed: 24982104]

2). Jaeken J, Matthijs G, Saudubray JM, Dionisi-Vici C, Bertini E, de Lonlay P, et al. Phosphomannose isomerase deficiency: a carbohydrate-deficient glycoprotein syndrome with hepatic-intestinal presentation. Am J Hum Genet 1998;62:1535–1539. [PubMed: 9585601]

3). de Lonlay P, Seta N. The clinical spectrum of phosphomannose isomerase deficiency, with an evaluation of mannose treatment for CDG-Ib. Biochim Biophys Acta 2009;1792:841–843. [PubMed: 19101627]

4). Niehues R, Hasilik M, Alton G, Korner C, Schiebe-Sukumar M, Koch HG, et al. Carbohydrate-deficient glycoprotein syndrome type Ib. Phosphomannose isomerase deficiency and mannose therapy. J Clin Invest 1998;101:1414–1420. [PubMed: 9525984]

5). Harms HK, Zimmer KP, Kurnik K, Bertele-Harms RM, Weidinger S, Reiter K. Oral mannose therapy persistently corrects the severe clinical symptoms and biochemical abnormalities of phosphomannose isomerase deficiency. Acta Paediatr 2002;91:1065–1072. [PubMed: 12434892]

6). Chu J, Mir A, Gao N, Rosa S, Monson C, Sharma V, et al. A zebrafish model of congenital disorders of glycosylation with phosphomannose isomerase deficiency reveals an early

opportunity for corrective mannose supplementation. Dis Model Mech 2013;6:95–105. [PubMed: 22899857]

7). Lee YA, Wallace MC, Friedman SL. Pathobiology of liver fibrosis: a translational success story. Gut 2015;64:830–841. [PubMed: 25681399]

8). Mudbhary R, Hoshida Y, Chernyavskaya Y, Jacob V, Villanueva A, Fiel MI, et al. UHRF1 overexpression drives DNA hypo-methylation and hepatocellular carcinoma. Cancer Cell 2014; 25:196–209. [PubMed: 24486181]

9). Yin C, Evas on KJ, Maher JJ, Stainier DY. The basic helix-loop-helix transcription factor, heart and neural crest derivatives expressed transcript 2, marks hepatic stellate cells in zebrafish: analysis of stellate cell entry into the developing liver. Hepatology 2012;56:1958–1970. [PubMed: 22488653]

10). Parsons MJ, Pisharath H, Yusuff S, Moore JC, Siekmann AF, Lawson N, Leach SD. Notch-responsive cells initiate the secondary transition in larval zebrafish pancreas. Mech Dev 2009;126:898–912. [PubMed: 19595765]

11). Chi NC, Shaw RM, De Val S, Kang G, Jan LY, Black BL, Stainier DY. Foxn4 directly regulates tbx2b expression and atrioventricular canal formation. Genes Dev 2008;22:734–739. [PubMed: 18347092]

12). Shtraizent N, DeRossi C, Nayar S, Sachidanandam R, Katz LS, Prince A, et al. MPI depletion enhances O-GlcNAcylation of p53 and suppresses the Warburg effect. Elife 2017;6:e22477.

13). Passeri MJ, Cinaroglu A, Gao C, Sadler KC. Hepatic steatosis in response to acute alcohol exposure in zebrafish requires sterol regulatory element binding protein activation. Hepatology 2009;49:443–452. [PubMed: 19127516]

14). Dimri M, Bilogan C, pierce LX, Naegele G, Vasanji A, Gibson I, et al. Three-dimensional structural analysis reveals a Cdk5-mediated kinase cascade regulating hepatic biliary network branching in zebrafish. Development 2017;144:2595–2605. [PubMed: 28720653]

15). Mederacke I, Hsu CC, Troeger JS, Huebener P, Mu X, Dapito DH, et al. Fate tracing reveals hepatic stellate cells as dominant contributors to liver fibrosis independent of its aetiology. Nat Commun 2013;4:2823. [PubMed: 24264436]

16). Xu L, Hui AY, Albanis E, Arthur MJ, O'Byrne SM, Blaner WS, et al. Human hepatic stellate cell lines, LX-1 and LX-2: new tools for analysis of hepatic fibrosis. Gut 2005;54:142–151. [PubMed: 15591520]

17). Shibata N, Watanabe T, Okitsu T, Sakaguchi M, Takesue M, Kunieda T, et al. Establishment of an immortalized human hepatic stellate cell line to develop antifibrotic therapies. Cell Transplant 2003;12:499–507. [PubMed: 12953924]

18). Moylan CA, Pang H, Dellinger A, Suzuki A, Garrett ME, Guy CD, et al. Hepatic gene expression profiles differentiate pre-symptomatic patients with mild versus severe nonalcoholic fatty liver disease. Hepatology 2014;59:471–482. [PubMed: 23913408]

19). Villanueva A, portela A, Sayols S, Battiston C, Hoshida Y, Mendez-Gonzalez J, et al. DNA methylation-based prognosis and epidrivers in hepatocellular carcinoma. Hepatology 2015;61:1945–1956. [PubMed: 25645722]

20). Subramanian A, Tamayo P, Mootha VK, Mukherjee S, Ebert BL, Gillette MA, et al. Gene set enrichment analysis: a knowledge-based approach for interpreting genome-wide expression profiles. Proc Natl Acad Sci U S A 2005;102:15545–15550. [PubMed: 16199517]

21). Ritchie ME, Phipson B, Wu D, Hu Y, Law CW, Shi W, Smyth GK. limma powers differential expression analyses for RNA-sequencing and microarray studies. Nucleic Acids Res 2015;43:e47.

22). Zhao XK, Yu L, Cheng ML, Che P, Lu YY, Zhang Q, et al. Focal adhesion kinase regulates hepatic stellate cell activation and liver fibrosis. Sci Rep 2017;7:4032. [PubMed: 28642549]

23). Goessling W, Sadler KC. Zebrafish: an important tool for liver disease research. Gastroenterology 2015;149:1361–1377. [PubMed: 26319012]

24). Zhang D, Golubkov VS, Han W, Correa RG, Zhou Y, Lee S, et al. Identification of Annexin A4 as a hepatopancreas factor involved in liver cell survival. Dev Biol 2014;395:96–110. [PubMed: 25176043]

25). Lorent K, Moore JC, Siekmann AF, Lawson N, Pack M. Reiterative use of the notch signal during zebrafish intrahepatic biliary development. Dev Dyn 2010;239:855–864. [PubMed: 20108354]

26). Zhang C, Ellis JL, Yin C. Inhibition of vascular endothelial growth factor signaling facilitates liver repair from acute ethanol-induced injury in zebrafish. Dis Model Mech 2016;9: 1383–1396. [PubMed: 27562099]

27). Friedman SL. Mechanisms of hepatic fibrogenesis. Gastroenterology 2008;134:1655–1669. [PubMed: 18471545]

28). Yang L, Jung Y, Omenetti A, Witek RP, Choi S, Vandongen HM, et al. Fate-mapping evidence that hepatic stellate cells are epithelial progenitors in adult mouse livers. Stem Cells 2008; 26:2104–2113. [PubMed: 18511600]

29). Hernandez-Gea V, Hilscher M, Rozenfeld R, Lim MP, Nieto N, Werner S, et al. Endoplasmic reticulum stress induces fibrogenic activity in hepatic stellate cells through autophagy. J Hepatol 2013;59:98–104. [PubMed: 23485523]

30). Chen Y, Choi SS, Michelotti GA, Chan IS, Swiderska-Syn M, Karaca GF, et al. Hedgehog controls hepatic stellate cell fate by regulating metabolism. Gastroenterology 2012;143:1319–1329.e11. [PubMed: 22885334]

31). Du K, Hyun J, Premont RT, Choi SS, Michelotti GA, Swiderska-Syn M, et al. Hedgehog-YAP signaling pathway regulates glutaminolysis to control activation of hepatic stellate cells. Gastroenterology 2018;154:1465–1479.e13. [PubMed: 29305935]

32). Tsuchida T, Friedman SL. Mechanisms of hepatic stellate cell activation. Nat Rev Gastroenterol Hepatol 2017;14:397–411. [PubMed: 28487545]

33). Lecca MR, Maag C, Berger EG, Hennet T. Fibrotic response in fibroblasts from congenital disorders of glycosylation. J Cell Mol Med 2011;15:1788–1796. [PubMed: 21029365]

34). Kocabayoglu P, Lade A, Lee YA, Dragomir AC, Sun X, Fiel MI, et al. beta-PDGF receptor expressed by hepatic stellate cells regulates fibrosis in murine liver injury, but not carcinogenesis. J Hepatol 2015;63:141–147. [PubMed: 25678385]

35). Kaetzel DM Jr, Morgan D III, Reid JD IV, Fenstermaker RA. Site-directed mutagenesis of the N-linked glycosylation site in platelet-derived growth factor B-chain results in diminished intracellular retention. Biochim Biophys Acta 1996;1298:250–260. [PubMed: 8980650]

36). Gonzalez PS, O'Prey J, Cardaci S, Barthet VJ, Sakamaki JI, Beaumatin F, et al. Mannose impairs tumour growth and enhances chemotherapy. Nature 2018;563:719–723. [PubMed: 30464341]

37). Sharma V, Smolin J, Nayak J, Ayala JE, Scott DA, Peterson SN, Freeze HH. Mannose alters gut microbiome, prevents diet-induced obesity, and improves host metabolism. Cell Rep 2018;24:3087–3098. [PubMed: 30231992]

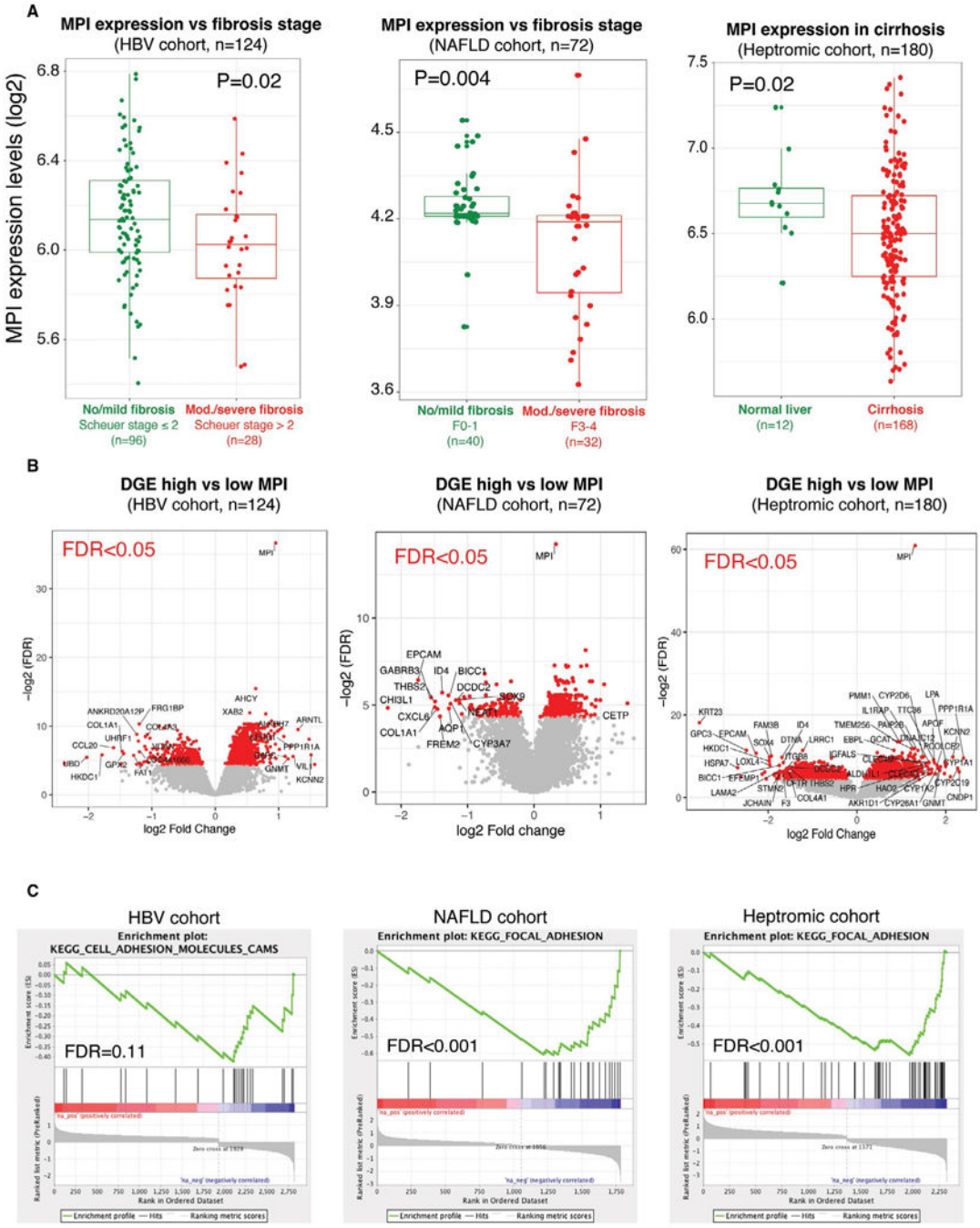

FIG. 1.

MPI expression is decreased in human liver samples with more advanced fibrosis. (A) Box plots for *MPI* expression in samples with advanced degree of fibrosis (red) versus milder or normal phenotypes (green). Analysis conducted in three different data sets with genome-wide genomic data available. (B) Volcano plots of genes differentially expressed among samples above and below the 90th and 10th percentile, respectively, of *MPI* expression. (C) Enrichment plots of the top-ranked gene sets significantly enriched between samples with

high and low *MPI* gene expression in the three data sets. Abbreviations: DGE, differential gene expression.

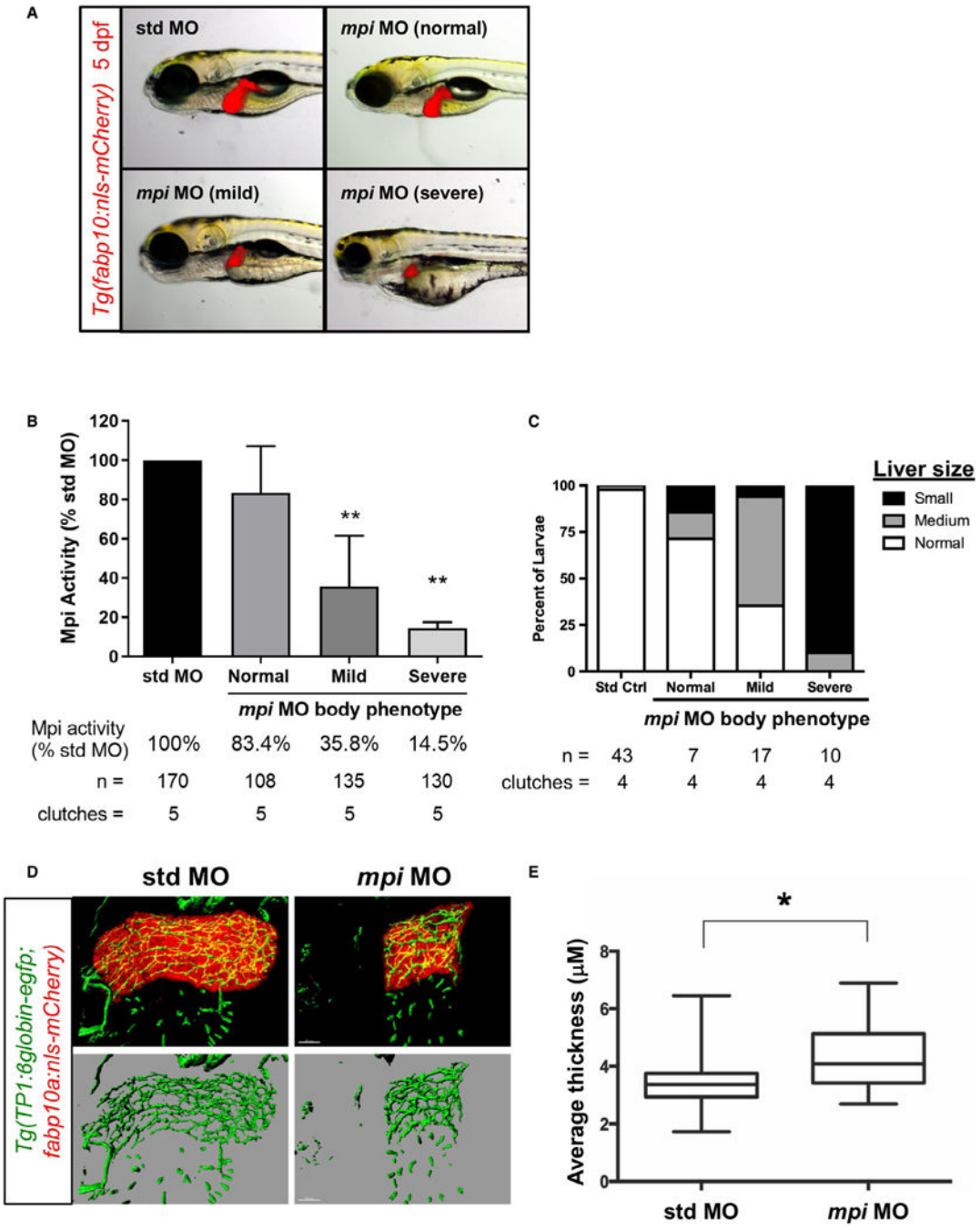

FIG. 2.

mpi morphant zebrafish have defects in liver development. (A) Overlay of fluorescent and bright-field images of 5 dpf *Tg(fabp10:nls-mCherry)* zebrafish larvae injected with standard control or *mpi* morpholino. Representative images, liver shown in red. (B) Mpi activity measurements from pooled 5-dpf zebrafish larvae separated into gross body phenotype groups as indicated, and reported as percent residual activity relative to standard (std) MO controls as mean ± SD from five independent clutches. $^{**}P < 0.01$. (C) Liver size correlates with severity of gross body phenotype (classification previously described in detail in Chu et

al.[6]). (D) Reconstruction of biliary epithelium in 5-dpf *mpi* morphant and control (siblings) *Tg(fabp10:nls-mcherry; TP1:βiglobin-egfp)* larvae. N = 3 per group. Representative images. (E) Biliary branches in *mpi* morphants were dilated when compared to controls. $*P < 0.05$, N = 3 standard control, 3 *mpi* morphant larvae.

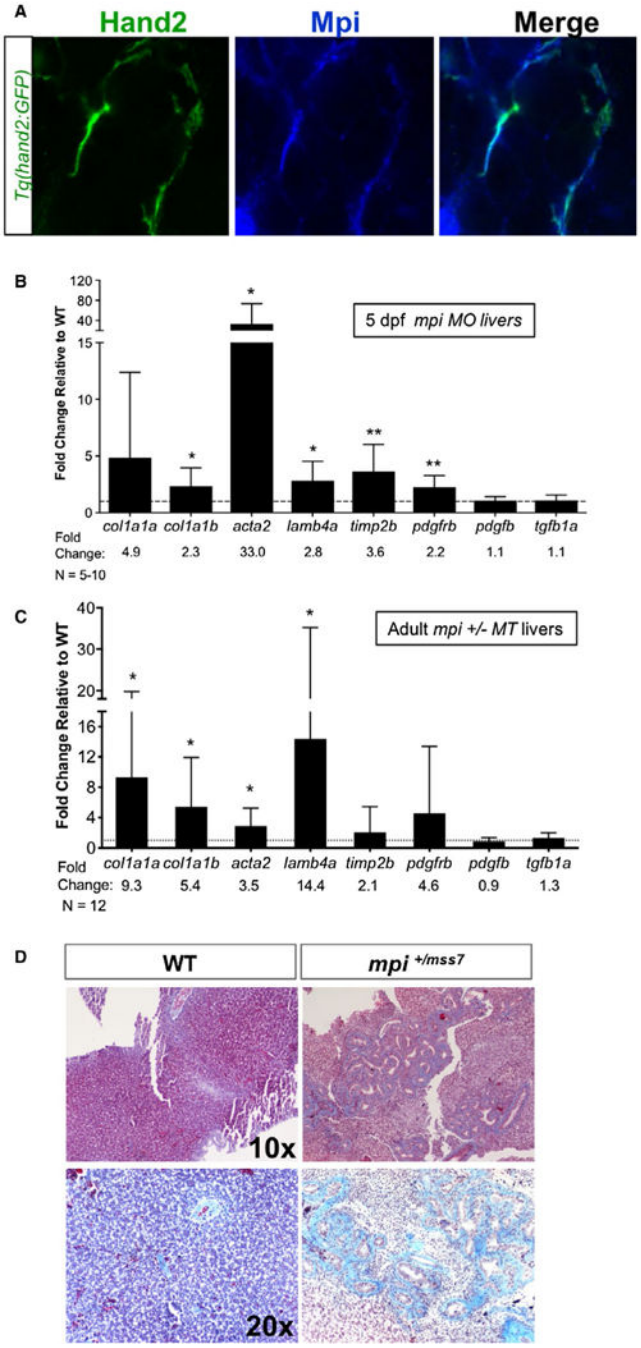

FIG. 3.

MPI depletion induces fibrotic gene expression and fibrosis in zebrafish liver. (A) Immunofluorescent staining for zebrafish Mpi (blue) in 5-dpf *Tg(hand2:EGFP)* larvae. Images are representative stainings from at least two independent samples. (B) qRT-PCR on whole-liver cDNA from 5-dpf control and *mpi* morphant larvae. Statistical significance was determined by unpaired Student *t* test (**P* < 0.05; ***P* < 0.01; N = 5–10 clutches analyzed per gene). Data are presented as mean ± standard deviation. (C) qRT-PCR on whole-liver cDNA prepped from adult WT (N = 9) and *mpi*$^{+/mss7}$ MT (N = 12) zebrafish. Statistical

significance was determined by unpaired Student *t* test (**P* < 0.05). Data are presented as mean ± standard deviation. (D) Representative images of Masson trichrome staining on paraffin-embedded whole-liver sections prepped from adult male WT (N = 5) and *mpi*$^{+/mss7}$ MT zebrafish (N = 4). Abbreviation: ctrl, control.

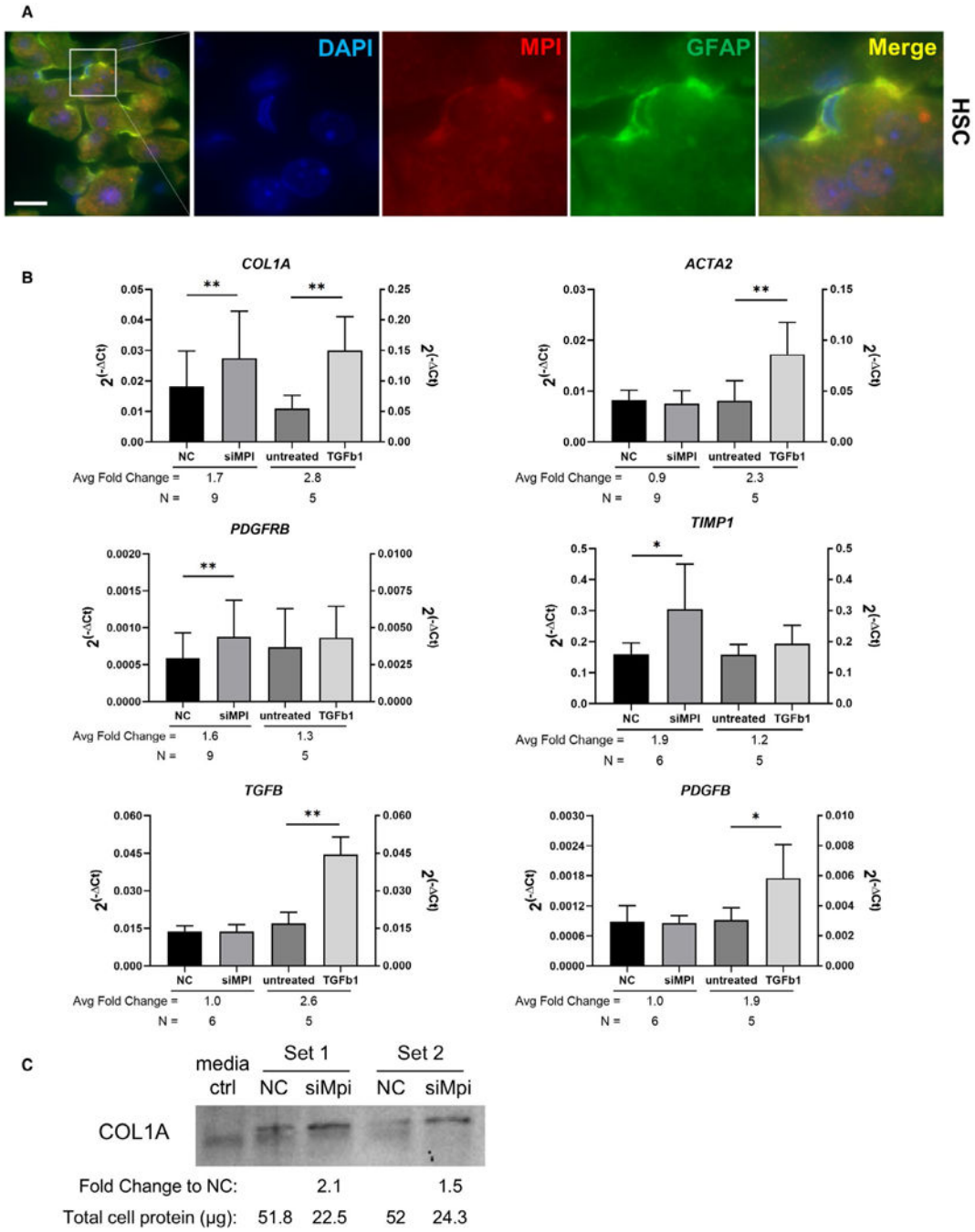

FIG. 4.

MPI depletion induces fibrotic gene expression. (A) Immunofluorescence staining in WT mouse liver for MPI and GFAP (HSC marker). Scale bar indicates 20 µM. Small outline in first panel represent magnified area. (B) qRT-PCR from siNC and siMPI LX-2 cDNA. Statistical significance was determined by paired Student *t* test (**P* < 0.05; ***P* < 0.01; n = 5–9 independent tranfection experiments per gene, as indicated). Data are presented as mean ± standard deviation. (C) Western blotting analysis demonstrating Collagen 1A secretion into conditioned media collected from LX-2 cells transfected with siNC or siMPI. Shown

are two independent sets of experiments, representative of five total experiments and with 2% FBS media as nonconditioned media control. Twenty microliters of TCA-precipitated media used per lane. Fold change in secreted COL1A signal intensity (relative NC controls) are shown, and total cell protein (μg) at time of collection are indicated. Abbreviations: NC, non-targeting control; *TIMP1,* tissue inhibitor of matrix metalloproteinase 1.

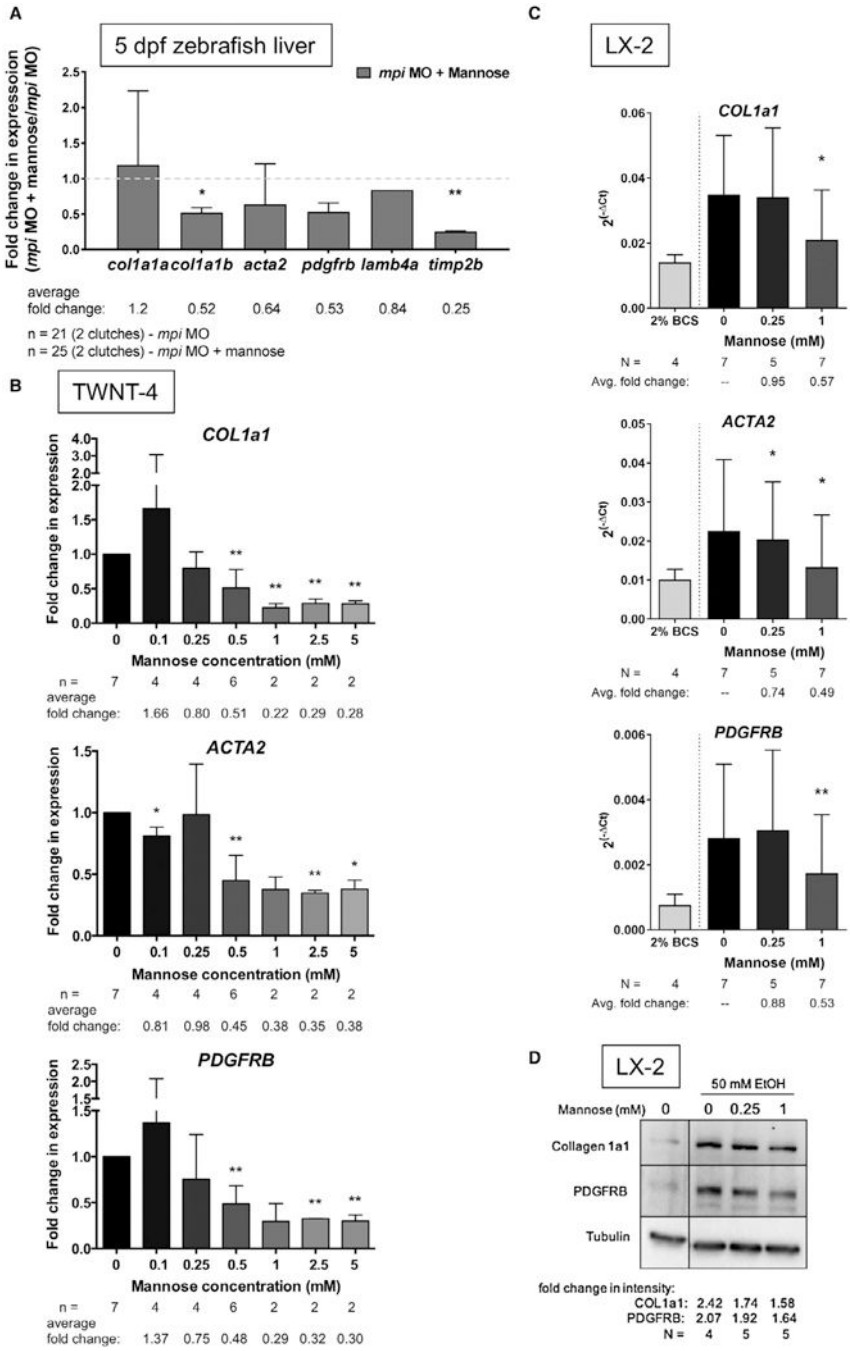

FIG. 5.

Mannose mitigates fibrotic gene expression. (A) qRT-PCR on liver cDNA prepared from 5 dpf control and *mpi* morphant ± 50 mM of mannose. Data are presented as fold change of *mpi* MO + 50 mM of mannose/*mpi* MO samples (N = 2). (B,C) qRT-PCR on cDNA from TWNT-4 cells (B) or 2% BCS or serum-activated LX-2 cells (C) treated with increasing concentrations of mannose. (D) Western blotting analysis of LX-2 cells following 24-hour serum starvation, then exposure to 50 mM of ethanol for 24 hours in the absence or presence of mannose. Band intensity quantified with ImageJ (NIH, Bethesda, MD), normalized to

Tubulin. Average fold change compared to untreated samples is indicated. Statistical significance shown in (A–C) determined by paired Student *t* test, $*P < 0.05$; $**P < 0.01$. Abbreviations: BCS, bovine calf serum; EtOH, ethanol.

Table 1.

Differentially Regulated pathway Analysis of Total proteins and phosphoproteins in Mannose-Treated Versus Control Human HSCs

Pathway name	Count	Wilcox_P
Total Protein		
KEGG_ALANINE_ASPARTATE_AND_GLUTAMATE_METABOLISM	8	0.0054
KEGG_GAP_JUNCTION	19	0.0056
KEGG_GLUTATHIONE_METABOLISM	14	0.0135
KEGG_FOLATE_BIOSYNTHESIS	3	0.0466
Phosphoprotein		
KEGG_VIRAL_MYOCARDITIS	8	0.0017
KEGG_GAP_JUNCTION	9	0.0174
KEGG_GLYCOLYSIS_GLUCONEOGENESIS	5	0.0182
KEGG_VASCULAR_SMOOTH_MUSCLE_CONTRACTION	9	0.0212
KEGG_MELANOGENESIS	7	0.0229